

Review



Article submitted to journal

Subject Areas:

cosmology, astrophysics

Keywords:isotropy, galaxy clusters, bulk flow,
cosmology, Hubble constant**Author for correspondence:**

Konstantinos Migkas

e-mail: kmigkas@strw.leidenuniv.nlGalaxy clusters as probes of
cosmic isotropyKonstantinos Migkas^{1,2}¹Leiden Observatory, Leiden University, PO Box 9513,
2300 RA Leiden, the Netherlands²SRON Netherlands Institute for Space Research,
Niels Bohrweg 4, NL-2333 CA Leiden, the Netherlands

Scaling relations of galaxy clusters are a powerful probe of cosmic isotropy in the late Universe. Owing to their strong cosmological dependence, galaxy cluster scaling relations can obtain tight constraints on the spatial variation of cosmological parameters, such as the Hubble constant (H_0), and detect large-scale bulk flow motions. Such tests are crucial to scrutinise the validity of Λ CDM in the local Universe and determine at what cosmic scales (if any) extragalactic objects converge to isotropy within the Cosmic Microwave Background rest frame. This review describes the methodology for conducting cosmic isotropy tests with cluster scaling relations and examines possible systematic biases. We also discuss the results of past studies that reported statistically significant observed anisotropies in the local Universe. Finally, we explore the future potential of cluster scaling relations as a cosmic isotropy probe given the large amount of multi-wavelength cluster data expected in the near future.

1. Introduction

The Cosmological Principle (CP) postulates that the Universe is statistically isotropic and homogeneous over sufficiently large scales. The primary experimental evidence for this assumption comes from Cosmic Microwave Background (CMB) observations [1]. CMB data support the existence of a rest frame (the so-called CMB rest frame) in which cosmic radiation in the very early Universe was highly isotropic. To reach this rest frame, one needs to remove the main anisotropic feature of the CMB; the well-known, dominant CMB dipole. The latter is presumed to arise due to our peculiar motion as observers within the CMB rest frame and the Doppler effect. Adopting the fully kinematic nature of the CMB dipole, one concludes our Solar system moves with 370 km/s towards the Galactic coordinates $(l, b) \approx (264^\circ, +48^\circ)$ within the CMB rest frame [2].

© The Authors. Published by the Royal Society under the terms of the Creative Commons Attribution License <http://creativecommons.org/licenses/by/4.0/>, which permits unrestricted use, provided the original author and source are credited.

The adoption of the CP in observational cosmology implies that cosmic matter in the late, low- z Universe should share the same rest frame as radiation in the early, high- z Universe. In other words, extra-galactic objects, such as galaxies, galaxy clusters, and supernovae (SN), should converge to statistical isotropy within the CMB rest frame when large cosmic volumes are considered. However, the CP alone does not define the scale at which convergence to isotropy should be achieved. For this, one needs individual cosmological models that predict the level of apparent anisotropy as a function of scale, as different models return different predictions. Hence, when one scrutinises the apparent (an)isotropy of the local Universe, one essentially tests the validity of specific cosmological models, and not the CP itself.

If a cosmological model is intrinsically isotropic, apparent anisotropies might emerge from unaccounted bulk flow motions.¹ Such bulk flows can bias the inference of the Hubble flow z_{Hubble} (the notation $z \equiv z_{\text{Hubble}}$ will be used hereafter) from the measured z_{obs} if the true peculiar velocities are not accurately known or not accounted for. Subsequently, the inferred cosmological distance from z will also be biased. The properties of bulk flows strongly depend on the degree of matter homogeneity at each cosmic scale. Consequently, the bulk flow amplitude as a function of scale varies for different models.

The standard cosmological model, Λ CDM, predicts that at ≥ 200 Mpc scales bulk flows should dissipate to ≤ 140 km/s (e.g., [3]). If such bulk flows are ignored, they can result in an observed $\leq 3\%$ anisotropy in the redshift-distance relation and the Hubble constant (H_0) within the CMB rest frame. Subsequently, larger apparent H_0 anisotropies or bulk flows at ≥ 200 Mpc scales would pose a challenge for Λ CDM. Interestingly, several studies have reported such observed anisotropies at $z \leq 0.06 - 0.2$, providing indications that the matter rest frame might not converge to the CMB rest frame at ≥ 200 Mpc (e.g., [3–14]). On the other hand, only a few of these findings exhibit sufficiently high statistical significance, while most are at only mild tension ($\leq 3\sigma$) with Λ CDM. As a result, the consistency of the local Universe kinematics with Λ CDM remains rather ambiguous and a topic of ongoing debate. Thus, it is crucial to develop novel, powerful techniques to scrutinise the assumption of isotropy in the late Universe and conclusively test the validity of Λ CDM at local scales.

2. Galaxy clusters as probes of local Universe isotropy

Galaxy clusters are one of the best probes to trace the isotropy of the redshift-distance relation at $\sim 200 - 2000$ Mpc ($z \sim 0.05 - 0.5$) scales. Clusters are uniformly distributed across the entire extra-galactic sky while we have high-quality data for thousands of clusters at these cosmic scales. In contrast, full-sky galaxy surveys are typically restricted to $z \leq 0.1$ scales (e.g., [15]). Moreover, although SNIa samples (e.g., [16]) cover a wide range of distances ($z \sim 0.01 - 1.5$), they suffer from strongly inhomogeneous sky distributions that can bias isotropy studies (e.g., [13]). As a result, galaxy clusters currently offer the best option for studying bulk flows and cosmological anisotropies at $z \sim 0.05 - 0.5$ scales, where, according to Λ CDM, extra-galactic objects should behave isotropically within the CMB rest frame.

(a) Cosmology-dependent cluster properties

A key element of galaxy clusters is that they are observed across most of the electromagnetic spectrum. Thus, numerous multi-wavelength cluster quantities can be determined independently. For instance, in X-rays, the hot ionised cluster gas is detected by its bremsstrahlung continuum and line emission. This allows one to measure the cluster's X-ray luminosity (L_X), gas mass (M_{gas}), and X-ray isophotal radius ($R_{50\%}$). In optical and infrared frequencies, one can examine the galaxy population of clusters and estimate the luminosity of the brightest central galaxy (L_{BCG}). Employing optical weak lensing data, the total cluster mass (M_{tot}) can also be estimated. In microwave frequencies, the total integrated Compton parameter (Y_{SZ} , equivalent to the total cluster gas pressure) is measured using the thermal Sunyaev-Zeldovich effect. The latter is caused by the inverse Compton scattering of CMB photons as they travel through the hot cluster gas.

¹The average peculiar velocity of a given cosmic volume, estimated by the peculiar velocities of individual extra-galactic objects within this volume.

The above-mentioned cluster properties can only be estimated with knowledge of the cluster's distance. However, an absolute calibration of cluster distances has yet to be available. Hence, assuming a Λ CDM Universe, one can infer the cluster's distance from its z as

$$D_L(z) = \frac{c(1+z)}{H_0} \int_0^z \frac{dz'}{E(z')} \quad \text{and} \quad D_A(z) = \frac{D_L(z)}{(1+z)^2}, \quad (2.1)$$

where $D_L(z)$ and $D_A(z)$ are the luminosity distance and angular diameter distance respectively, c is the speed of light, $E(z) = \sqrt{\Omega_m(1+z)^3 + \Omega_\Lambda}$ is the normalised Hubble parameter, and Ω_m and Ω_Λ are the normalised matter and dark energy densities respectively. As a result, the inference of these galaxy cluster properties from observables strongly depends on the fiducial H_0 value, making such cluster properties *cosmology-dependent*. Moreover, the inference of z , and consequently $D_L(z)$ and $D_A(z)$, depends on the observed z_{obs} and the peculiar velocity z_{pec} as:

$$1 + z_{\text{obs}} = (1+z)(1+z_{\text{pec}}). \quad (2.2)$$

Thus, bulk flows can bias the cluster distance if the former are ignored, i.e., it is assumed that $z_{\text{obs}} \approx z$. This bias then propagates to all cosmology-dependent cluster properties.

(b) Cosmology-independent cluster properties

The key cluster property to test cosmic isotropy is the gas temperature (T_X). The latter is observationally determined through X-ray spectroscopy and its measurement does not depend on cosmological parameters or peculiar velocities.² Therefore, T_X is *cosmology-independent*. T_X is a measure of the kinetic energy of the gas and reflects the depth of the cluster's gravitational well. The latter is also traced by the kinetic energy of the galaxies, which is characterised by the galaxy velocity dispersion σ_{vel} , measured in optical/infrared wavelengths. σ_{vel} is also determined without any cosmological assumptions and can be an alternative to T_X as a cosmology-independent cluster property to be used for testing cosmic isotropy. Finally, the optical richness of galaxy clusters (λ) is another useful cosmology-independent quantity for isotropy tests.

(c) Galaxy cluster scaling relations

All the multi-wavelength cluster properties mentioned above scale with the total cluster mass. As a result, they scale with each other, giving rise to the so-called *galaxy cluster scaling relations*. Most such relations are theoretically motivated (see e.g., [18]) and have been established observationally for at least two decades (see [19,20] for a review on galaxy cluster scaling relations). They are described by single power laws that in logarithmic space take the form:

$$\log Y + C_{YX} \log E(z) = A_{YX} + B_{YX} \log X \pm \sigma_{\text{intr},YX} \quad (2.3)$$

where Y and X are the two scaling cluster properties, A_{YX} , B_{YX} , and $\sigma_{\text{intr},YX}$ are respectively the intercept, slope, and intrinsic scatter of the $Y-X$ scaling relation, and C_{YX} , together with the $\log E(z)$ term, account for the redshift evolution of the relation. When one uses a cosmology-dependent and cosmology-independent cluster property as Y and X , the cosmological dependence of such a scaling relation maximises. For example, let us consider the $L_X - T_X$ relation (Fig. 1). We know that $L_X = 4\pi D_L(z) \times K_{\text{corr}} f_X$, where f_X is the observed X-ray cluster flux and K_{corr} is the K-correction that converts the L_X from the observer's rest frame to the cluster's rest frame. Therefore, Eq. 2.3 can be written as

$$\log f_X + 2 \log D_L(z) + C_{LT} \log E(z) + \log(4\pi K_{\text{corr}}) = A_{LT} + B_{LT} \log T_X \pm \sigma_{\text{intr},LT}. \quad (2.4)$$

All terms that include $E(z)$ and numerical constants can be summarised into a single term $G(\Omega_m, C_{LT}, z)$.³ Eq. 2.4 can be then rewritten separating the cosmology-dependent and cosmology-independent terms:

$$2 \log H_0 + A_{LT} + G(\Omega_m, C_{LT}, z) = \log f_X - B_{LT} \log T_X \pm \sigma_{\text{intr},LT}. \quad (2.5)$$

²The only cosmological dependency of the T_X measurement comes from the selection of the cluster spectra extraction region which usually depends on first estimating the radius of the cluster. However, the final T_X dependency on H_0 is $T_X \sim H_0^{-0.07}$ (see Appendix B in [17]). The T_X dependency on bulk flows is similarly weak (see Appendix E.4 in [17]).

³ $G(\Omega_m, C_{LT}, z) = 2 \log \left[c(1+z) \int_0^z \frac{dz'}{E(z')} \right] + C_{LT} \log E(z) + \log(4\pi K_{\text{corr}})$

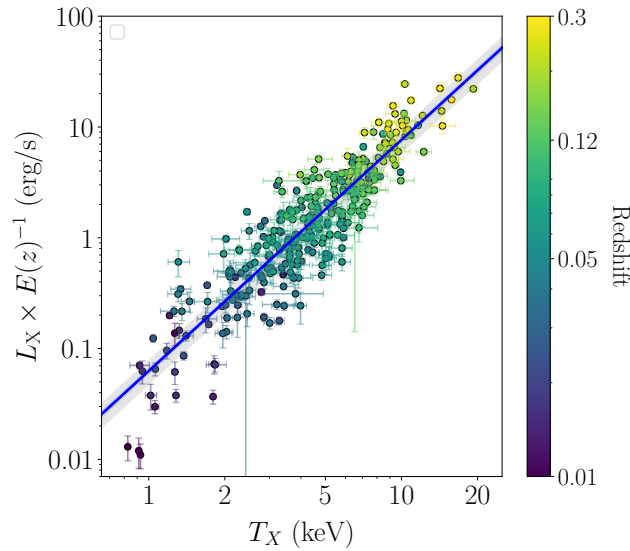


Figure 1: $L_X - T_X$ scaling relation for the 313 clusters presented in [21] and [17]. The colour of data points corresponds to the cluster redshift. The blue and grey shaded areas represent the statistical and total scatter, respectively.

On the right side of Eq. 2.5, f_X and T_X are observables and directly measured quantities. On the contrary, B_{LT} and $\sigma_{\text{intr},LT}$ are nearly completely insensitive to cosmological changes. On the left side of Eq. 2.5, there is strong cosmological dependence due to the $2 \log H_0$ and $G(\Omega_m, C_{LT}, z)$ terms. The intercept A_{LT} is not a cosmological quantity but it is completely degenerated with H_0 since A_{LT} is not known independently of cosmological assumptions.

(d) Testing cosmological parameter isotropy and bulk flows

In an isotropic Universe, the best-fit $2 \log H_0 + A_{LT} + G(\Omega_m, C_{LT}, z)$ sum should not spatially vary. One can scrutinise the isotropy hypothesis and investigate the directionality of cosmological parameters (e.g., H_0) and bulk flows by constraining Eq. 2.5 in independent sky patches. To do so, sufficiently large and uniform cluster samples should be employed. Such an approach reveals how much each sky direction deviates from the average, all-sky behaviour. This deviation can then be translated to the necessary variation of cosmological parameters to reconcile each direction with the rest of the sky. This approach does not assume the anisotropy shape. Alternatively, one can fit Eq. 2.5 to the full, all-sky cluster sample while introducing an anisotropic component with an assumed shape in the scaling relation model, e.g., a dipole anisotropy. In this case, the extra free parameters are the direction and amplitude of the anisotropy. Each approach can be applied to different z bins to characterise any retrieved anisotropy as a function of cosmic scale. As explained in Sect. i, ii, and iii, using different z bins one can eventually distinguish H_0 and Ω_m anisotropies, as well as bulk flows since these cosmological phenomena impact the observed anisotropy of Eq. 2.5 differently. Thus, the degeneracy between the individual left-side terms of Eq. 2.5 can be broken and one can draw conclusions on individual cosmological parameters.

Every cluster scaling relation can be decomposed to observables and cosmological parameters as in Eq. 2.5. Each time, the cosmological sensitivity of the scaling relation changes according to how the utilised cluster properties depend on cosmic distance. For example, $M_{\text{gas}} \propto D_A^{\frac{5}{2}}$; as a result, the $M_{\text{gas}} - T_X$ relation leads to the strongest H_0 dependence with $2.5 \log H_0$.⁴ Similarly, the $R_{50\%} - T_X$ relation leads to a $\log H_0$ dependence. Furthermore, one can study scaling relations between two cosmology-dependent properties

⁴The dependence on Ω_m and other parameters through G is more complicated and also depends on the redshift evolution of the relation as explained in Sect. iii

and still see some residual cosmology dependence. The latter depends on B_{YX} as well. For instance, the $L_X - M_{\text{gas}}$ relation shows $B_{LM_{\text{gas}}} \sim 1.2$ (e.g., [22,23]), which results in a $\sim \log H_0$ dependence. One can apply the same exercise to any scaling relation.

It is evident from the above that, using just one galaxy cluster sample with multiple measured quantities per cluster, one can obtain complementary information on cosmic isotropy. The different isotropy constraints also yield excellent consistency checks and reveal possible systematic and cluster physics biases, further reinforcing the robustness of the methodology. The plethora of (nearly independent) cosmological information given per object constitutes a substantial advantage of clusters as probes of cosmic isotropy over other extra-galactic objects.

(i) H_0 anisotropies

The dominant cosmological effect in Eq. 2.5 and other similar scaling relations comes from the $N_{YX} \log H_0$ term. N_{YX} varies according to the used scaling relation, as explained before. Absolute constraints can be put on the sum $N_{YX} \log H_0 + A_{YX}$ but not on H_0 alone without assuming the value of A_{YX} . However, A_{YX} is not expected to vary with direction. A_{YX} depends on inner-cluster (mostly baryonic) physics, such as cluster gas thermodynamics, and the mechanisms that connect the scaling cluster properties. Thus, the true, "intrinsic" A_{YX} is independent of the spacetime between the cluster and the observer. As a result, A_{YX} carries no information about the redshift-distance relation. Assuming that clusters are locally described by the same physical laws, A_{YX} should not have any directional dependence, i.e., it should be statistically isotropic. Thus, when statistically significant angular variations of $N_{YX} \log H_0 + A_{YX}$ are observed, the bulk of the effect can be attributed to an H_0 anisotropy. In practice, one keeps A_{YX} fixed and treats H_0 as a free parameter across the sky. As explained above, the absolute H_0 values are arbitrary and depend on the exact choice of A_{YX} ; for example, A_{YX} can be chosen so the full-sky cluster sample returns $H_0 = 70$ km/s/Mpc. On the other hand, relative angular H_0 variations are directly constrained and are completely independent of the assumed A_{YX} value.

Finally, an angular variation of H_0 is degenerate with bulk flows at $z \lesssim 0.1$ scales and almost entirely independent of bulk flows at $z \gtrsim 0.2$ (see Sect. ii). On the other hand, there is strong degeneracy between H_0 and Ω_m anisotropies at $z \gtrsim 0.4$ while there is almost none at $z \lesssim 0.2$ (see Sect. iii). Thus, at $z \approx 0.2 - 0.3$, one can purely trace H_0 anisotropies with no strong effects from other possible cosmological anisotropies. At more local or distant scales, one can independently trace anisotropies on the redshift-distance relation as a whole. However, to attribute such an apparent anisotropy to an individual cosmological parameter (or bulk flow), one needs to assume the other degenerate cosmological parameter to be fixed or vary within a limited range.

(ii) Bulk flows

Bulk flows can have a substantial impact on the directional behavior of $G(\Omega_m, C_{YX}, z)$ and scaling relations. Bulk flows can affect the inference of z due to large (unaccounted) cluster peculiar velocities with non-negligible z_{pec} compared to z (Eq. 2.2). Such effects are mostly relevant for local cluster samples ($z \lesssim 0.15$). For higher- z clusters peculiar velocities become irrelevant compared to the Hubble recession velocity. In essence, even if strong bulk flows exist at $z \gtrsim 0.2$, they will not cause any detectable anisotropy to scaling relations.

A biased z due to bulk flow presence strongly affects the inferred cluster distance through the integration limits of $\int_0^z \frac{dz'}{E(z')}$. At the same time, it leaves $E(z)$ nearly unaffected, constituting the exact redshift evolution term $C_{YX} \log E(z)$ insignificant for bulk flow studies. As an example, a +1000 km/s bulk flow at $z = 0.05$ would cause a $\approx 7\%$ overestimation of $\int_0^z \frac{dz'}{E(z')}$ and only a $< 0.2\%$ change in $E(z)$. As previously mentioned, bulk flows at $z \lesssim 0.2$ scales have similar effects on scaling relations as an H_0 angular variation. For example, a 7% H_0 anisotropy would also cause a 7% change in the inferred cluster distance, having the same effect with a +1000 km/s bulk flow at $z = 0.05$. Consequently, one cannot easily distinguish between the two phenomena at local scales. Nevertheless, when more distant clusters are studied, the effect of bulk flows fades out while an H_0 anisotropy has the same effect for every cosmic scale. Characteristically, the same +1000 km/s bulk flow would only cause a 1.6% change in D_L at $z = 0.2$.

(iii) Ω_m , Ω_Λ , and w anisotropies

An angular variation of the $E(z)$ factor (i.e., Ω_m , Ω_Λ , and the dark energy equation-of-state w) will cause an anisotropic effect on $G(\Omega_m, C_{YX}, z)$ under certain conditions. For local cluster samples ($z \lesssim 0.3$), $E(z)$ variations only weakly affect the directional behaviour of most scaling relations, usually on a lower level than statistical noise. At higher- z , directional variations in $E(z)$ become more impacting on $G(\Omega_m, C_{YX}, z)$ and can be detected above the statistical noise level. $E(z)$ affects $G(\Omega_m, C_{YX}, z)$ through both $\log \left[\int_0^z \frac{dz'}{E(z')} \right]$ and $C_{YX} \log E(z)$. However, for scaling relations with $C_{YX} > 0$ (e.g., $Y_{SZ} - T_X$ and $M_{\text{gas}} - T_X$), changes in $E(z)$ tend to partially cancel out between the two terms, suppressing the impact of an $E(z)$ anisotropy on scaling relations even at high- z . On the other hand, for scaling relations with $C_{YX} < 0$ (e.g., $L_X - T_X$), the impact of $E(z)$ on $G(\Omega_m, C_{YX}, z)$ is enhanced. Consequently, by studying the anisotropic behaviour of $C_{YX} < 0$ and $C_{YX} > 0$ scaling relations, it is trivial to conclusively distinguish between an $E(z)$ anisotropy and a bulk flow or an H_0 anisotropy (for which C_{YX} is irrelevant). The value of C_{YX} can either assumed to be known from the self-similar model [18], adopted from a past study that constrained it (e.g., [24]), or treat it as a free parameter. Nonetheless, as mentioned before, the effects of $E(z)$ anisotropies remain small for $z \lesssim 0.3$ samples for any C_{YX} . For now, there is very limited availability of adequately large, all-sky, high- z cluster samples with which $E(z)$ anisotropies could be studied.

Changes in Ω_m could also cause a directional dependence of the true A_{YX} and B_{YX} values for scaling relations between properties that trace the total amount of gas (e.g., L_X) and the total cluster mass (e.g., M_{tot} or even T_X), due to the different gas fraction per direction. These additional effects might be challenging to take into account. For all these reasons, the cosmological parameters included in $E(z)$ are often assumed to be fixed and any observed anisotropies are attributed to H_0 variations or bulk flows which have a much stronger influence at $z \lesssim 0.3$ clusters anyway.

(iv) When cluster physics effects and systematic biases dominate

There are scaling relations that exhibit negligible cosmological dependence and can be utilised to detect systematic biases or cluster physics effects. These relations are particularly helpful for disentangling the signal from the possible cosmological anisotropies from other cluster-related causes that might influence the conclusions on isotropy. For example, the $L_X - Y_{SZ}$ relation has $B_{LY} \sim 0.93$ [17] which results in a $\lesssim 0.1 \log H_0$ dependency. Consequently, the $L_X - Y_{SZ}$ relation is insensitive to cosmological anisotropies. However, it can effectively trace biases in the X-ray Galactic absorption correction applied to L_X . While the latter is subject to Galactic absorption effects, Y_{SZ} is not since it is measured in microwaves. Thus, a statistically significant angular variation of $L_X - Y_{SZ}$ can provide the true X-ray absorption per direction by revealing a systematic over- or underestimation of the relative correction factor for different sky patches. Similarly, the $R_{50\%} - M_{\text{gas}}$ relation yields a rather weak $0.4 \log H_0$ dependency (Migkas et al. in prep.). Hence, its angular variation level is mainly dictated by the average morphology of the cluster population per direction. Cluster morphology (e.g., relaxed or disturbed and cool core or non-cool core) strongly affects $R_{50\%}$ while it does not cause considerable changes to M_{gas} . Therefore, it is essential to robustly check if the cosmological sensitivity of a scaling relation is higher than its sensitivity on different cluster physics effects and systematics before we conduct isotropy tests.

(e) Properties of cluster samples used for isotropy tests

To carry out an unbiased test of cosmic isotropy using galaxy cluster samples, the latter should ideally fulfil certain criteria. Firstly, a similar cluster population across the sky is needed. This ensures that A_{YX} is similar in every direction. A homogeneous cluster selection, independent of direction, generally achieves such a cluster population uniformity. It also provides similar numbers of clusters in every direction, allowing for balanced full-sky coverage, which is a necessity for an accurate isotropy test. Even if a sample is not uniformly built, one can apply selection cuts to obtain a uniform cluster population across different sky patches before conducting isotropy tests.

If a cluster sample is constructed with an inhomogeneous selection, the sample might suffer from a directional dependence on cluster properties. For instance, more relaxed/disturbed clusters or more intrinsically brighter/fainter clusters may be found in a specific direction than the rest of the sky. Such an

imbalance in the average cluster properties will cause an anisotropic A_{YX} since distinct cluster populations are described by somewhat different scaling relations. If one ignores the spatial variation of A_{YX} , the inferred cosmological anisotropy will be overestimated. However, even in a homogeneously selected cluster sample, A_{YX} can slightly vary across the sky due to the random variations of the cluster population. That is, A_{YX} can slightly vary across the sky due to statistical noise. This effect is small for low-scattered scaling relations, but it should (and can) be taken into account when inferring the angular variation of cosmological parameters. If it is assumed to be negligible, it might lead to an overestimation of the apparent cosmological anisotropies.

Another useful feature of cluster samples used for cosmic isotropy studies is the similarity of the z distribution across the sky. This serves two purposes. Firstly, if an inaccurate C_{YX} value is adopted and a rather high- z sample is studied, a dissimilar z distribution will induce directional biases in the scaling relation parameters. These could be wrongfully interpreted as cosmological anisotropies. On the contrary, if the z distribution is consistent across the sky, a wrong C_{YX} value will cause the same bias towards every direction, which will eventually cancel out when comparing independent sky regions; that is, the cosmological anisotropy constraints will remain unaffected. Nevertheless, for local cluster samples ($z \lesssim 0.2$), C_{YX} biases become insignificant since no strong cluster evolution is expected in such a local cosmic volume. The second reason why a similar z is essential is that, when comparing cosmological parameters across different sky patches, one wishes to trace similar cosmic volumes. Let us assume a hypothetical anisotropy is present only at, e.g., $z \lesssim 0.1$ due to bulk flows. Then, if clusters in one direction lie at greater distances on average, they will not be affected by such a bulk flow. On the other hand, if more local clusters are found in a different direction, they will be affected by the bulk flow. This will bias the detection of such a cosmological effect.

3. Evidence for local anisotropy from galaxy clusters

(a) First application and preliminary findings

Probing cosmic isotropy with galaxy cluster scaling relations is a relatively new sub-field of cosmology. The idea was introduced in [25] where they used the $L_X - T_X$ relation to test cosmic isotropy with two independent cluster samples; the ASCA Cluster Catalog (ACC, [26]) and the first data release of the XMM Cluster Survey sample (XCS, [27]). ACC is an archival sample containing 272 clusters with a rather uniform sky distribution and median $z \approx 0.09$. XCS was built from archival *XMM-Newton* data and contains 364 with L_X and T_X measurements. These clusters cover the full sky but not uniformly, with some regions having many more objects than others. XCS is a rather high- z sample with median $z \approx 0.35$. [25] performed a 1D analysis with respect to the Galactic longitude l measuring H_0 and Ω_m across different l bins. Interestingly, they identified the same anisotropy patterns in both cluster samples despite the latter being independent while tracing different cosmic scales. They found H_0 to vary by $\sim 20\%$ at a mild $\approx 2.5 - 3\sigma$ level, with the discrepancy being more prominent at $z \lesssim 0.35$. This analysis offered a first glance at the potential of cluster scaling relations as proxies of cosmic isotropy; nonetheless, the results were preliminary since both used samples suffered from certain weaknesses. For example, ACC was compiled by old, low-quality X-ray cluster measurements with no specific selection. Also, T_X was measured within a non-physical cluster radius. On the other hand, XCS composed of low-mass galaxy clusters and groups that generally suffer from larger scaling relation dispersion. Also, the T_X was measured with large uncertainty in a radius that strongly depended on the fiducial cosmology (within 300 kpc from the cluster's center); several clusters also had photometric z instead of spectroscopic. Finally, both samples did not have sufficient information to robustly assess the cluster population characteristics per direction. Thus, there was still much room for progressing this methodology.

(b) First 2D results and improved cluster catalogues

Results on apparent H_0 variations from the $L_X - T_X$ scaling relation were significantly improved by [21]. That study presented and utilised an X-ray flux-limited, homogeneously-selected local cluster sample, namely, a preliminary version of the extremely expanded HIGH FLUX Galaxy Cluster Sample (eeHIFLUGCSv0). The latter consists of 313 clusters with self-consistently measured, high-quality T_X

measurements with low statistical uncertainties as obtained using deep *XMM-Newton* and *Chandra* data. The 313 clusters cover the full sky uniformly and have a median $z \approx 0.075$ while almost all clusters lie at $z \lesssim 0.3$. The $L_X - T_X$ scatter was shown to be much lower for eeHIFLUGCSv0 than ACC and XCS. Adequate information to characterise the cluster population per direction was also provided. Moreover, [21] implemented cones of varying angular sizes covering all directions in the sky, providing the first 2D results on apparent H_0 variations from cluster scaling relations. For eeHIFLUGCSv0, they identified a $\approx 13\%$ H_0 maximum angular variation with a statistical significance of 3.59σ towards $(l, b) \sim (281^\circ, -16^\circ)$. This finding was consistent with the directions identified by [25]. The anisotropy was also present when $z < 0.03$ clusters were excluded, suggesting that the bulk of the effect continues beyond $\gtrsim 130$ Mpc. Jointly analysing the 842 independent cluster samples from eeHIFLUGCSv0, ACC, and XCS, [21] found a combined $\approx 14\%$ apparent H_0 variation towards $(l, b) \sim (312^\circ, -21^\circ)$ at a 4.55σ level. However, this finding did not assume the shape of the anisotropy as they simply compared the two most extreme, independent sky regions. When a dipole anisotropy was assumed, the H_0 variation and statistical significance dropped to $\approx 11\%$ 4σ level, respectively. [21] explored an extensive list of possible systematic biases but failed to identify any bias that would alleviate the tension with the isotropy hypothesis. Overall, this work confirmed the strong indications for an anisotropy in the late Universe, as traced by galaxy clusters. Nevertheless, further confirmation was needed and remaining systematics were still to be addressed.

(c) More precise results from multi-wavelength cluster scaling relations

The most robust evidence for a local Universe anisotropy using galaxy clusters was presented by [17]. In that study, they used the eeHIFLUGCSv0 sample as presented in [21] and additionally measured the microwave Y_{SZ} , infrared L_{BCG} , and X-ray $R_{50\%}$ for each cluster using *Planck*, 2MASS, and *ROSAT* data respectively. They also measured Y_{SZ} for the ACC sample. These new measurements allowed the construction of ten multi-wavelength scaling relations. The statistical methodology was also noticeably improved compared to past studies. Combining all the available information by properly accounting for all scatter and measurement covariance, [17] detected an apparent 9% H_0 dipole anisotropy towards $(l, b) \sim (280^\circ, -15^\circ)$ at an unprecedented 5.4σ level (displayed in Fig. 2). They assessed the statistical significance of the H_0 dipole by employing isotropic Monte Carlo simulations. Furthermore, [17] fully exploited 14 cosmology-independent cluster properties (e.g., relaxation state, Galactic absorption, metallicity, exposure time, and cluster core T_X) to predict the expected H_0 behaviour of a cluster sub-sample purely based on cluster population criteria. This sophisticated approach confirmed that the emerging H_0 dipole is not significantly affected by cluster population differences across the sky. Overall, numerous tests were performed to ensure the validity of their results.

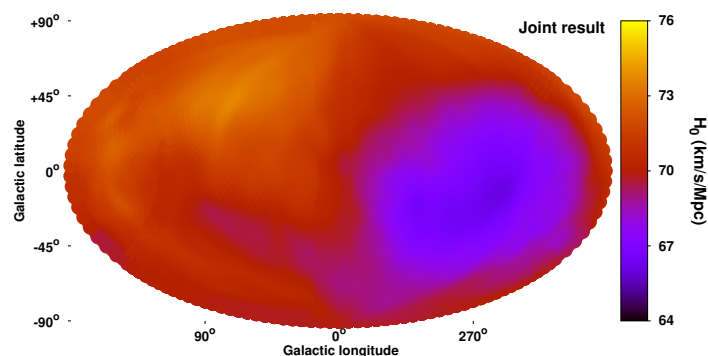


Figure 2: H_0 anisotropy map as derived by [17] from the joint analysis of different multiwavelength scaling relations and cluster samples. A 9% H_0 dipole was detected with a statistical significance of 5.4σ (credit: Migkas et al., 2021, A&A, 649, A151).

Since eeHIFLUGCSv0 is a local cluster sample, one can attribute the apparent H_0 anisotropy to large cluster bulk flow. As explained in Sect. ii, the two cosmological effects are nearly indistinguishable at $z \lesssim 0.2$. [17] explored this scenario and provided the first bulk flow constraints from galaxy cluster scaling relations. They found that the apparent H_0 dipole could emerge due to a $\approx 900 \pm 200$ km/s bulk flow extending beyond 500 Mpc ($z \gtrsim 0.12$). As displayed in Fig. 3, they constrained the cluster bulk flow as a function of different cosmic volumes and shells. Different scaling relations and independent cluster samples returned consistent results with the best-fit bulk flow amplitude ranging from $\sim 600 - 1200$ km/s. They found that the bulk flow direction did not significantly deviate within $z \sim 0.05 - 0.15$ scales. However, they noted that the results beyond $z \gtrsim 0.1$ are likely overestimated as they are dominated by lower- z objects. However, there is no available comparison with another independent study yet since galaxy clusters are the only probes for now that cover these cosmic scales uniformly across the sky. Overall, this study provided the strongest evidence until now that the cluster rest frame does not coincide with the CMB rest frame at $z \lesssim 0.15$, which is in strong contrast with Λ CDM.

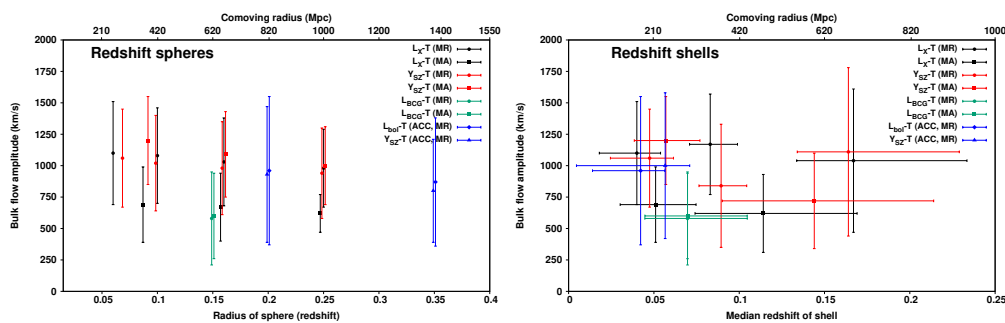


Figure 3: *Left*: Bulk flow amplitude and its 1σ uncertainty as a function of the redshift (or comoving distance) radius as determined by [17]. The results from different scaling relations, cluster samples, and statistical approaches are displayed in different shapes and colours. *Right*: Same as left panel but as a function of redshift (or comoving distance) shells instead of spheres (credit: Migkas et al., 2021, A&A, 649, A151).

It is important to note that the 5.4σ statistical significance of the apparent H_0 dipole detection in [17] does not directly correspond to the tension with Λ CDM. The latter still allows for limited residual anisotropy due to bulk flow motions at these scales. For ~ 500 Mpc volumes ($z \lesssim 0.12$), Λ CDM predicts an average ≈ 80 km/s bulk flow which roughly corresponds to a $\sim 1\%$ dipole H_0 anisotropy. Consequently, the findings of [17] are at a $\sim 4.5\sigma$ tension with Λ CDM. Finally, they fixed A_{YX} for all scaling relations; this might underestimate the H_0 dipole uncertainty. However, the final statistical significance is not expected to be overestimated since they follow the same procedure using isotropic Monte Carlo simulations.

To conclude, past studies using various multi-wavelength scaling relations and independent cluster samples strongly and consistently indicate an apparent H_0 angular variation within $\lesssim 1$ Gpc. However, the apparent anisotropy can be alleviated by a considerable cluster bulk flow motion, although the latter is in notable tension with Λ CDM as well. Future studies with new data and further improved methodologies will reveal if the observed dipole anisotropy truly constitutes a remarkable failure of the standard cosmological model in the local Universe or if its statistical significance has been overestimated.

4. Future Outlook

We live in the era of next-generation, state-of-the-art cosmological surveys that remarkably increase the amount of available data and aim at precise cosmological constraints. Furthermore, recent hydrodynamical cosmological simulations offer a unique tool to help us better understand observational findings and uncover potential systematic biases. As a result, there is vast potential for scrutinising cosmic isotropy with galaxy clusters using various approaches. Moreover, new advances in the statistical and modelling methodology

might offer new valuable insights. Here we present a non-exhaustive list of expected future advances in this sub-field that will yield significant results within the next years.

(a) New cluster data from multi-wavelength surveys

There are numerous cosmological experiments that will soon provide (or have already done so) valuable new cluster data. First and foremost, the extended ROentgen Survey with an Imaging Telescope Array (*eROSITA*, [28]) and its planned 4-year *eROSITA* All-Sky Survey (eRASS) will substantially progress cluster science owing to the largest X-ray cluster catalogues ever compiled. Already from the first all-sky scan (eRASS1), *eROSITA* has detected > 12,000 X-ray clusters, with > 8,000 of them as new detections [29]. Almost all of these clusters have L_X and M_{gas} measurements, while for ~ 450 of them, precise T_X measurements are already available.⁵ These numbers will significantly increase as deeper eRASS data are analysed, reaching $\geq 50,000$ massive clusters for eRASS:8 [31]. Additionally, 1499 eRASS1 clusters have σ_{vel} measurements [32] that will allow the study of X-ray-optical scaling relations, such as $L_X - \sigma_{\text{vel}}$. Due to the large amount of new X-ray cluster information *eROSITA* will return, a significant improvement in cosmic isotropy tests with X-ray clusters is expected.

In the optical and infrared regime, the *Euclid* telescope and its *Euclid* Wide Survey will scan $\approx 15,000^\circ$ in the extra-galactic sky, discovering $\geq 10^5$ massive clusters ($M_{\text{tot}} \geq 2 \times 10^{14} M_\odot$) at $z > 0.2$ [33]. Additionally, $\geq 10^4$ of these clusters will be at $z > 1.3$. For a large fraction of them, *Euclid* will measure σ_{vel} and λ values, as well as M_{tot} through weak lensing data. This will allow for constructing optical cluster scaling relations with vast numbers of used objects. As a result, *Euclid* will allow for an unprecedented characterisation of isotropy at large cosmic scales, insensitive to local effects, such as bulk flows. Other optical surveys that (will) cover large areas of the sky, such as the ones from *Rubin* Observatory and *DESI*, will also detect tens and hundreds of thousands of clusters, respectively, measuring useful optical properties for many of them [34–36]. It is evident that the abundance of optical galaxy cluster information to become available in the next years is striking and will immensely advance our understanding of cosmic isotropy at large scales.

In microwave, the Atacama Cosmology Telescope (*ACT*) has already provided > 4000 SZ-detected clusters with Y_{SZ} measurements and a median $z \approx 0.5$ [37]. *ACT* significantly increased the availability of Y_{SZ} values compared to past cluster samples. The efficiency of X-ray-SZ scaling relations for testing cosmic isotropy was demonstrated in [17]. Finally, this list is non-exhaustive since many more cosmological experiments will provide valuable cluster data in the near future.

(b) Low-scattered scaling relations and improved modelling

There are two primary approaches to improve constraints on cosmic isotropy; firstly, employ new, larger samples as outlined in Sect. (a), and secondly, reduce the scaling relation scatter of current samples. The constraining power roughly scales with $\sim \delta / \sqrt{N}$, where δ is a relation's dispersion (or scatter) and N is the number of used objects. Hence, lowering the scatter of a scaling relation to half has the same constraining effect as increasing the sample size by a factor of four. Consequently, it is evident that suppressing the scatter of current scaling relations with improved modelling is highly important.

Certain scaling relations with lower scatter than those utilised in past studies are expected to return valuable insights in the near future. For example, the $M_{\text{gas}} - T_X$ scaling relation is particularly useful for cosmic isotropy tests due to its low H_0 dispersion ($\delta_{H_0} \approx 11\%$). Moreover, the $L_X - T_X$ relation (and other X-ray relations) exhibits significantly reduced scatter when the core-excised L_X is used instead of the total L_X [38]. Hence, core-excised cluster measurements can be implemented to improve existing isotropy results. Furthermore, cluster morphology parameters, such as the X-ray concentration and centroid shift, correlate with the scatter of some scaling relations [39–41]. A similar scatter correlation has been found with the cluster dynamical state [17,42–44]. If one measures the cluster morphology and includes it in the scaling relation model, this could potentially reduce the scatter and enhance the cosmological constraints.

⁵*eROSITA* T_X measurements were recently found to deviate from T_X measured by other major X-ray telescopes, such as *Chandra* and *XMM-Newton* [30]. However, this deviation is accurately known and one can correct for it, not jeopardising isotropy tests with *eROSITA* T_X measurements.

(c) Cosmological simulations

The validity of methodologies that search for apparent, statistically significant cosmic anisotropies should be cross-checked using cosmological simulations. Recently, the state-of-the-art hydrodynamical FLAMINGO simulations were introduced [45]. FLAMINGO recreates different realisations of isotropic Λ CDM universes with $\sim 10^9 M_{\odot}$ mass resolution and implements full baryonic physics effects. The simulations also provide lightcones for multiple different observers reaching out to 2.8 Gpc ($z \sim 0.8$) and for different cosmologies. Numerous properties for each simulated halo are available for each lightcone, including all the cluster properties discussed in this review. As a result, different methods for detecting cosmic anisotropies can be applied to the FLAMINGO data to investigate the robustness of each method. Such a test will also assess the true rarity of the observed anisotropies within a Λ CDM universe.

5. Discussion and Summary

Galaxy clusters and their scaling relations offer an extraordinary tool for probing cosmic isotropy at a wide range of cosmic scales. For now, galaxy clusters are the only isotropy probe for which we have uniform, all-sky data at $z \sim 0.05 - 0.5$. Moreover, clusters have a unique advantage over other isotropy probes; they can provide information on the angular variation of cosmological parameters across many different wavelengths. This enables the construction of numerous multi-wavelength scaling relations that probe cosmic isotropy almost independently, with only a single cluster sample. Low-scattered scaling relations between cosmology-dependent (e.g., L_X , Y_{SZ} , and M_{gas}) and cosmology-independent (e.g., T_X and σ_{vel}) cluster properties are exceptionally useful for such tests. Nonetheless, every scaling relation can be decomposed into observables and cosmological parameters. Thus, by determining the angular variation of each scaling relation, robust conclusions on the anisotropy of cosmological parameters and the existence of large-scale bulk flows can be drawn. Angular H_0 variations identically affect all cosmic scales, while bulk flows and Ω_m anisotropies mainly affect $z \leq 0.2$ and $z \geq 0.3$ scales, respectively. Scaling relations that are insensitive to cosmological anisotropies (e.g., $L_X - Y_{SZ}$ and $R_{50\%} - M_{\text{gas}}$) can reveal multiple directional cluster physics effects and help us isolate the cosmological signal from such potential biases.

There are, however, certain pitfalls in this method. The most critical is that the used sample should show a similar cluster population throughout the sky. Varying cluster populations (e.g., relaxed or disturbed, low or high mass, and centrally peaked or diffuse) are often (but not always) described by slightly different scaling relations. A uniform cluster selection that results in similar cluster populations is essential to ensure that the underlying scaling relations of the independent cluster sub-samples are statistically equivalent. Thus, any observed difference can be then attributed to cosmological effects. If there are variations in the cluster population between compared regions, the inference of any cosmological effect can be distorted. Correspondingly, compared cluster sub-samples must also have comparable z distributions to make certain we trace the same cosmic scales per direction.

Recent studies used several multi-wavelength cluster scaling relations to probe the isotropy of the local ($z \leq 0.3$) Universe. Specifically, [17] reported the detection of a $9.0 \pm 1.7\%$ H_0 dipole using X-ray, SZ, and infrared cluster data, substantially challenging the convergence to isotropy hypothesis at these cosmic scales. They argued that the apparent H_0 variation might be caused by a ~ 900 km/s cluster bulk flow extending to 500 Mpc, at $\geq 4\sigma$ tension with Λ CDM.

New cluster samples of unprecedented sizes from current and future surveys will considerably boost the cosmic isotropy constraints from scaling relations. Such surveys include *eROSITA* and *Euclid* that will eventually measure X-ray and optical/infrared cluster quantities for $\geq 50,000$ and $\geq 10^5$ clusters, respectively. Moreover, improvements in scaling relations can be achieved by considering the cluster morphology and dynamical state. Such refined modelling will result in lower scatter and more precise cosmological constraints.

Finally, utilising large, cosmological, hydrodynamical simulations will enable testing the robustness of different anisotropy detection methods using cluster scaling relations. This is crucial in order to understand the importance of the observational findings, eliminating possible systematic biases in the applied methodology. Overall, multi-wavelength galaxy cluster scaling relations will play a pivotal role in testing the isotropy of the late Universe in the near future.

Acknowledgements. I acknowledge support in the form of the X-ray Oort Fellowship at Leiden Observatory. I would also like to thank the Royal Society and the organisers for inviting me as a speaker to the "Challenging the standard cosmological model" meeting, which sparked the writing of this review. Finally, I thank my wife for taking several vacation days off her job to care for our son so I can finish writing this review on time.

References

1. Planck Collaboration, Akrami Y, Ashdown M, Aumont J, Baccigalupi C, Ballardini M, Banday AJ, Barreiro RB, Bartolo N, Basak S et al.. 2020a Planck 2018 results. VII. Isotropy and statistics of the CMB. *A&A* **641**, A7. ([10.1051/0004-6361/201935201](https://doi.org/10.1051/0004-6361/201935201))
2. Planck Collaboration, Aghanim N, Akrami Y, Arroja F, Ashdown M, Aumont J, Baccigalupi C, Ballardini M, Banday AJ, Barreiro RB, et al.. 2020b Planck 2018 results. I. Overview and the cosmological legacy of Planck. *A&A* **641**, A1. ([10.1051/0004-6361/201833880](https://doi.org/10.1051/0004-6361/201833880))
3. Watkins R, Allen T, Bradford CJ, Ramon A, Walker A, Feldman HA, Cionitti R, Al-Shorman Y, Kourkchi E, Tully RB. 2023 Analysing the large-scale bulk flow using cosmicflows4: increasing tension with the standard cosmological model. *MNRAS* **524**, 1885–1892. ([10.1093/mnras/stad1984](https://doi.org/10.1093/mnras/stad1984))
4. Colin J, Mohayaee R, Sarkar S, Shafieloo A. 2011 Probing the anisotropic local Universe and beyond with SNe Ia data. *MNRAS* **414**, 264–271. ([10.1111/j.1365-2966.2011.18402.x](https://doi.org/10.1111/j.1365-2966.2011.18402.x))
5. Carrick J, Turnbull SJ, Lavaux G, Hudson MJ. 2015 Cosmological parameters from the comparison of peculiar velocities with predictions from the 2M++ density field. *MNRAS* **450**, 317–332. ([10.1093/mnras/stv547](https://doi.org/10.1093/mnras/stv547))
6. Colin J, Mohayaee R, Rameez M, Sarkar S. 2019 Evidence for anisotropy of cosmic acceleration. *A&A* **631**, L13. ([10.1051/0004-6361/201936373](https://doi.org/10.1051/0004-6361/201936373))
7. Salehi A, Yarahmadi M, Fathi S, Bamba K. 2021 Cosmological bulk flow in the Λ CDM model: (in)consistency with Λ CDM. *MNRAS* **504**, 1304–1319. ([10.1093/mnras/stab909](https://doi.org/10.1093/mnras/stab909))
8. Mc Conville R, Ó Colgáin E. 2023 Anisotropic distance ladder in Pantheon+supernovae. *PRD* **108**, 123533. ([10.1103/PhysRevD.108.123533](https://doi.org/10.1103/PhysRevD.108.123533))
9. Cowell JA, Dhawan S, Macpherson HJ. 2023 Potential signature of a quadrupolar hubble expansion in Pantheon+supernovae. *MNRAS* **526**, 1482–1494. ([10.1093/mnras/stad2788](https://doi.org/10.1093/mnras/stad2788))
10. Sorrenti F, Durrer R, Kunz M. 2024 The low multipoles in the Pantheon+SH0ES data. *arXiv e-prints* p. arXiv:2403.17741. ([10.48550/arXiv.2403.17741](https://doi.org/10.48550/arXiv.2403.17741))
11. Whitford AM, Howlett C, Davis TM. 2023 Evaluating bulk flow estimators for CosmicFlows-4 measurements. *MNRAS* **526**, 3051–3071. ([10.1093/mnras/stad2764](https://doi.org/10.1093/mnras/stad2764))
12. Hoffman Y, Valade A, Libeskind NI, Sorce JG, Tully RB, Pfeifer S, Gottlöber S, Pomarède D. 2024 The large-scale velocity field from the Cosmicflows-4 data. *MNRAS* **527**, 3788–3805. ([10.1093/mnras/stad3433](https://doi.org/10.1093/mnras/stad3433))
13. Hu JP, Wang YY, Hu J, Wang FY. 2024 Testing the cosmological principle with the Pantheon+ sample and the region-fitting method. *A&A* **681**, A88. ([10.1051/0004-6361/202347121](https://doi.org/10.1051/0004-6361/202347121))
14. Yarahmadi M, Salehi A, Farajollahi H. 2024 Measuring cosmic bulk flow with Pantheon catalogue in perturbed $f(R)$ gravity. *MNRAS* **527**, 11840–11854. ([10.1093/mnras/stad3939](https://doi.org/10.1093/mnras/stad3939))
15. Tully RB, Kourkchi E, Courtois HM, Anand GS, Blakeslee JP, Brout D, Jaeger Td, Dupuy A, Guinet D, Howlett C, Jensen JB, Pomarède D, Rizzi L, Rubin D, Said K, Scolnic D, Stahl BE. 2023 Cosmicflows-4. *ApJ* **944**, 94. ([10.3847/1538-4357/ac94d8](https://doi.org/10.3847/1538-4357/ac94d8))
16. Scolnic D, Brout D, Carr A, Riess AG, Davis TM, Dwomoh A, Jones DO, Ali N, Charvu P, Chen R, et al.. 2022 The Pantheon+ Analysis: The Full Data Set and Light-curve Release. *ApJ* **938**, 113. ([10.3847/1538-4357/ac8b7a](https://doi.org/10.3847/1538-4357/ac8b7a))
17. Migkas K, Pacaud F, Schellenberger G, Erler J, Nguyen-Dang NT, Reiprich TH, Ramos-Ceja ME, Lovisari L. 2021 Cosmological implications of the anisotropy of ten galaxy cluster scaling relations. *A&A* **649**, A151. ([10.1051/0004-6361/202140296](https://doi.org/10.1051/0004-6361/202140296))
18. Kaiser N. 1986 Evolution and clustering of rich clusters.. *MNRAS* **222**, 323–345. ([10.1093/mnras/222.2.323](https://doi.org/10.1093/mnras/222.2.323))
19. Giodini S, Lovisari L, Pointecouteau E, Ettori S, Reiprich TH, Hoekstra H. 2013 Scaling Relations for Galaxy Clusters: Properties and Evolution. *SSR* **177**, 247–282. ([10.1007/s11214-013-9994-5](https://doi.org/10.1007/s11214-013-9994-5))
20. Lovisari L, Maughan BJ. 2022 Scaling Relations of Clusters and Groups and Their Evolution. In *Handbook of X-ray and Gamma-ray Astrophysics*, p. 65. ([10.1007/978-981-16-4544-0_118-1](https://doi.org/10.1007/978-981-16-4544-0_118-1))
21. Migkas K, Schellenberger G, Reiprich TH, Pacaud F, Ramos-Ceja ME, Lovisari L. 2020 Probing cosmic isotropy with a new X-ray galaxy cluster sample through the L_X -T scaling relation. *A&A* **636**, A15. ([10.1051/0004-6361/201936602](https://doi.org/10.1051/0004-6361/201936602))

22. Zhang YY, Andernach H, Caretta CA, Reiprich TH, Böhringer H, Puchwein E, Sijacki D, Girardi M. 2011 HIFLUGCS: Galaxy cluster scaling relations between X-ray luminosity, gas mass, cluster radius, and velocity dispersion. *A&A* **526**, A105. ([10.1051/0004-6361/201015830](https://doi.org/10.1051/0004-6361/201015830))
23. Lovisari L, Reiprich TH, Schellenberger G. 2015 Scaling properties of a complete X-ray selected galaxy group sample. *A&A* **573**, A118. ([10.1051/0004-6361/201423954](https://doi.org/10.1051/0004-6361/201423954))
24. Reichert A, Böhringer H, Fassbender R, Mühlegger M. 2011 Observational constraints on the redshift evolution of X-ray scaling relations of galaxy clusters out to $z \sim 1.5$. *A&A* **535**, A4. ([10.1051/0004-6361/201116861](https://doi.org/10.1051/0004-6361/201116861))
25. Migkas K, Reiprich TH. 2018 Anisotropy of the galaxy cluster X-ray luminosity-temperature relation. *A&A* **611**, A50. ([10.1051/0004-6361/201731222](https://doi.org/10.1051/0004-6361/201731222))
26. Horner DJ. 2001 *X-ray scaling laws for galaxy clusters and groups*. PhD thesis University of Maryland College Park.
27. Mehrrens N, Romer AK, Hilton M, Lloyd-Davies EJ, Miller CJ, Stanford SA, Hosmer M, Hoyle B, Collins CA, Liddle AR, et al.. 2012 The XMM Cluster Survey: optical analysis methodology and the first data release. *MNRAS* **423**, 1024–1052. ([10.1111/j.1365-2966.2012.20931.x](https://doi.org/10.1111/j.1365-2966.2012.20931.x))
28. Predehl P, Andritschke R, Arefiev V, Babyshkin V, Batanov O, Becker W, Böhringer H, Bogomolov A, Boller T, Borm K et al.. 2021 The eROSITA X-ray telescope on SRG. *A&A* **647**, A1. ([10.1051/0004-6361/202039313](https://doi.org/10.1051/0004-6361/202039313))
29. Bulbul E, Liu A, Kluge M, Zhang X, Sanders JS, Bahar YE, Ghirardini V, Artis E, Seppi R, Garrel C, et al.. 2024 The SRG/eROSITA All-Sky Survey. The first catalog of galaxy clusters and groups in the Western Galactic Hemisphere. *A&A* **685**, A106. ([10.1051/0004-6361/202348264](https://doi.org/10.1051/0004-6361/202348264))
30. Migkas K, Kox D, Schellenberger G, Veronica A, Pacaud F, Reiprich TH, Bahar YE, Balzer F, Bulbul E, Comparat J, et al.. 2024 The SRG/eROSITA All-Sky Survey: SRG/eROSITA cross-calibration with Chandra and XMM-Newton using galaxy cluster gas temperatures. *arXiv e-prints* p. arXiv:2401.17297. ([10.48550/arXiv.2401.17297](https://arxiv.org/abs/2401.17297))
31. Pillepich A, Porciani C, Reiprich TH. 2012 The X-ray cluster survey with eRosita: forecasts for cosmology, cluster physics and primordial non-Gaussianity. *MNRAS* **422**, 44–69. ([10.1111/j.1365-2966.2012.20443.x](https://doi.org/10.1111/j.1365-2966.2012.20443.x))
32. Kluge M, Comparat J, Liu A, Balzer F, Bulbul E, Ider Chitham J, Ghirardini V, Garrel C, Bahar YE, Artis E, et al.. 2024 The First SRG/eROSITA All-Sky Survey: Optical Identification and Properties of Galaxy Clusters and Groups in the Western Galactic Hemisphere. *arXiv e-prints* p. arXiv:2402.08453. ([10.48550/arXiv.2402.08453](https://arxiv.org/abs/2402.08453))
33. Sartoris B, Biviano A, Fedeli C, Bartlett JG, Borgani S, Costanzi M, Giocoli C, Moscardini L, Weller J, Ascaso B, Bardelli S, Maurogordato S, Viana PTP. 2016 Next generation cosmology: constraints from the Euclid galaxy cluster survey. *MNRAS* **459**, 1764–1780. ([10.1093/mnras/stw630](https://doi.org/10.1093/mnras/stw630))
34. Ivezić Ž, Kahn SM, Tyson JA, Abel B, Acosta E, Allsman R, Alonso D, AlSayyad Y, Anderson SF, Andrew J, et al.. 2019 LSST: From Science Drivers to Reference Design and Anticipated Data Products. *ApJ* **873**, 111. ([10.3847/1538-4357/ab042c](https://doi.org/10.3847/1538-4357/ab042c))
35. Zou H, Gao J, Xu X, Zhou X, Ma J, Zhou Z, Zhang T, Nie J, Wang J, Xue S. 2021 Galaxy Clusters from the DESI Legacy Imaging Surveys. I. Cluster Detection. *ApJs* **253**, 56. ([10.3847/1538-4365/abe5b0](https://doi.org/10.3847/1538-4365/abe5b0))
36. Wen ZL, Han JL. 2024 A catalog of 1.58 million clusters of galaxies identified from the DESI Legacy Imaging Surveys. *arXiv e-prints* p. arXiv:2404.02002. ([10.48550/arXiv.2404.02002](https://arxiv.org/abs/2404.02002))
37. Hilton M, Sifón C, Naess S, Madhavacheril M, Oguri M, Rozo E, Rykoff E, Abbott TMC, Adhikari S, Aguena M et al.. 2021 The Atacama Cosmology Telescope: A Catalog of >4000 Sunyaev-Zel'dovich Galaxy Clusters. *ApJs* **253**, 3. ([10.3847/1538-4365/abd023](https://doi.org/10.3847/1538-4365/abd023))
38. Pratt GW, Croston JH, Arnaud M, Böhringer H. 2009 Galaxy cluster X-ray luminosity scaling relations from a representative local sample (REXCESS). *A&A* **498**, 361–378. ([10.1051/0004-6361/200810994](https://doi.org/10.1051/0004-6361/200810994))
39. Bharadwaj V, Reiprich TH, Schellenberger G, Eckmiller HJ, Mittal R, Israel H. 2014 Intracluster medium cooling, AGN feedback, and brightest cluster galaxy properties of galaxy groups. Five properties where groups differ from clusters. *A&A* **572**, A46. ([10.1051/0004-6361/201322684](https://doi.org/10.1051/0004-6361/201322684))
40. Zhu Y, Wang YH, Zhao HH, Jia SM, Li CK, Chen Y. 2019 The $Y_{SZ,Planck} - Y_{SZ,XMM}$ scaling relation and its difference between cool-core and non-cool-core clusters. *Research in Astronomy and Astrophysics* **19**, 104. ([10.1088/1674-4527/19/7/104](https://doi.org/10.1088/1674-4527/19/7/104))
41. Yuan ZS, Han JL, Wen ZL. 2022 Dynamical state of galaxy clusters evaluated from X-ray images. *MNRAS* **513**, 3013–3021. ([10.1093/mnras/stac1037](https://doi.org/10.1093/mnras/stac1037))
42. Zhang YY, Reiprich TH, Schneider P, Clerc N, Merloni A, Schwobe A, Borm K, Andernach H, Caretta CA, Wu XP. 2017 HIFLUGCS: X-ray luminosity-dynamical mass relation and its implications for mass calibrations with the SPIDERS and 4MOST surveys. *A&A* **599**, A138. ([10.1051/0004-6361/201628971](https://doi.org/10.1051/0004-6361/201628971))

43. Lovisari L, Schellenberger G, Sereno M, Ettori S, Pratt GW, Forman WR, Jones C, Andrade-Santos F, Randall S, Kraft R. 2020 X-Ray Scaling Relations for a Representative Sample of Planck-selected Clusters Observed with XMM-Newton. *ApJ* **892**, 102. ([10.3847/1538-4357/ab7997](https://doi.org/10.3847/1538-4357/ab7997))
44. Poon H, Okabe N, Fukazawa Y, Akino D, Yang C. 2023 Scaling relations of X-ray luminous clusters in the Hyper Suprime-Cam Subaru Strategic Program field. *MNRAS* **520**, 6001–6016. ([10.1093/mnras/stad514](https://doi.org/10.1093/mnras/stad514))
45. Schaye J, Kugel R, Schaller M, Helly JC, Braspenning J, Elbers W, McCarthy IG, van Daalen MP, Vandenbroucke B, Frenk CS, et al.. 2023 The FLAMINGO project: cosmological hydrodynamical simulations for large-scale structure and galaxy cluster surveys. *MNRAS* **526**, 4978–5020. ([10.1093/mnras/stad2419](https://doi.org/10.1093/mnras/stad2419))